

Constructing Polycrystalline Hybrid Ternary CuS/Co₃O₄ with Supported Graphitic Nitride Electrocatalyst for Bifunctional Water Splitting Reactions

Imtiaz Ahmed^a Zahir Abbas^a and Shaikh M. Mobin^{*,ab}

^aDepartment of Chemistry, Indian Institute of Technology Indore, Simrol Khandwa Road, 433552, India.

^bCenter for Advanced Electronics (CAE), Indian Institute of Technology Indore, Simrol Khandwa Road, 433552, India.

* E-mail: xray@iiti.ac.in

<i>Sr. No</i>	<i>Contents</i>	<i>Page</i>
1.	Instrumentations	S3
2.	Experimental Section	S3-4
3.	Table S1 PXRD Rietveld refined structural information of Co ₃ O ₄ , CuS, binary composite and ternary composite system.	S4-6
4.	Fig. S1: (a-c) FESEM images of CuS pristine materials.	S6
5.	Fig. S2: (a-c) FESEM images of Co ₃ O ₄ pristine materials.	S6
6.	Fig. S3: ATR-FTIR spectra of ternary, binary and pristine Co ₃ O ₄ , CuS and g-C ₃ N ₄ .	S7
7.	Fig. S4. XPS survey spectra of ternary nanostructure.	S7
8.	Table S2. Mass activity results of ternary binary composite and all other pristine electrocatalyst.	S7
9.	Electrochemical surface area:	S8
10.	Fig. S5. Cyclic voltammetry curves of (a) pristine Co ₃ O ₄ (b) pristine CuS (c) g-C ₃ N ₄ composite (d-f) are their corresponding plot of J _a and J _c against scan rate for the determination of double layer capacitance (C _{dl}) of the catalysts, respectively.	S8

11.	Fig. S6. ECSA Normalization from LSV in 1M KOH for OER.	S9
12.	Fig. S7. TOF from LSV at voltage of 1.70 V of ternary, binary, Co_3O_4 CuS and g- C_3N_4 only in 1M KOH for OER.	S9
13.	Fig. S8. CV curves of ternary, binary, Co_3O_4 , CuS and g- C_3N_4 in 1 M KOH (pH ~ 13.8) solution in a given potential range of 0.2 V to 0.3 V (vs RHE) at a scan rate of 40 mV/s to enumerate the active sites.	S10
14.	Table S3. Active sites (τ) and TOF results of ternary binary, Co_3O_4 , CuS and g- C_3N_4 electrocatalyst.	S10
15.	Table S4. Comparison of OER and HER activity of ternary nanostructure with some reported copper and cobalt based catalysts in an alkaline medium and acidic medium.	S11-12
16.	Table S5. Comparison of OER and HER chrono and LSV stability of some reported copper and cobalt based catalysts in an alkaline medium and acidic medium.	S12
17.	Fig. S9: Polarization curves (LSV) plot, representing the overpotential at higher current density (100 mA/cm ²) for both (a) HER and (b) OER for the electrocatalyst.	S13
18.	Most Possible Overall HER pathway:	S13
19.	Most Possible Overall OER pathway:	S14
20.	Fig. S10: Post catalytic XRD and FESEM analysis of ternary electrocatalyst after chronoamperometric stability test in 1 M KOH.	S14
21.	Fig. S11: Post catalytic mapping analysis of ternary electrocatalyst after chronoamperometric stability test in 1 M KOH.	S15
22.	Fig. S12: Post catalytic FTIR analysis of ternary electrocatalyst after chronoamperometric stability test in 1 M KOH.	S 15
23.	Reference	S16

Instrumentation:

All the reagents and solvents were purchased from a commercial source without any further purification. For the Powder X-ray diffraction (PXRD) analysis Cu K α (0.154 nm) monochromatic radiation was used with a Rigaku Smart Lab X-ray diffractometer. X-ray photoelectron spectroscopy (XPS) measurements were carried out with a Kratos Axis Ultra system, equipped with a monochromatic AlK α X-ray source. The survey spectra were measured with 80 eV pass energy and 1 eV step size whereas with the high-resolution spectra 20 eV pass energy and 100 mV step size was used. All XPS measurements were performed using the charge neutralizer. The morphologies were investigated by a Supra55 Zeiss field emission scanning electron microscope (FESEM) and high-resolution transmission electron microscopy (HR-TEM) was performed using (TEM, JEM F200) at an operating voltage of 300 kV. The attenuated total reflectance Fourier transform infrared (ATR-FTIR) spectra were recorded with a Bruker Alpha II system over the wavenumber range of 4000–400 cm⁻¹. All electrochemical measurements were performed with Metrohm Autolab (PGSTAT-204N) single channel potentiostat/galvanostat using NOVA 2.1.5 setup software.

EXPERIMENTAL SECTION

Materials: Copper (II) chloride (CuCl₂) were obtained SRL, Cobalt (II) nitrate hexahydrate (Co(NO₃)₂·6H₂O), ethanol (AR grade 99.9%), potassium hydroxide (AR grade KOH), Thiourea (CS(NH₂)₂) and melamine (C₃N₃(NH₂)₃) were obtained from Spectrochem. 5% Nafion™ 117 solution IrO₂ and Pt/C and was bought from Sigma-Aldrich. Carbon cloth was purchased from Global-Tech India Pvt Ltd. for electrode preparation. The compounds were kept in a desiccated location and utilized without subsequent purification.

Synthesis Procedure of CuS: Synthesis of pristine CuS was carried out by preparing two different suspensions, 0.51g (3.69 mmol.) in 10 mL of ethylene glycol in a glass beaker with stirring to form solution I and thiourea 0.5 g (6.57 mmol.) in 15 ml DI H₂O in another beaker to form solution II. Solution II was slowly dropped into solution I with continuous stirring and kept the reaction mixture under continuous stirring for 30 min at 40 °C. The entire reaction mixture was transferred into a Teflon-lined stainless-steel autoclave and subjected to a hydrothermal reaction at 160°C for 12 hours. After the reaction, the resulting product was washed multiple times with deionized water (DI H₂O) and ethanol to remove any impurities. Finally, the obtained sample was kept on drying for overnight at 70 °C and then used for further

binary and ternary material synthesis. The schematic representation of the synthesis procedure for the flower-shaped CuS is illustrated in Scheme 1.

Synthesis procedure of Co₃O₄: To prepare Co₃O₄, 727.5 mg of cobalt nitrate hexahydrate (Co(NO₃)₂·6H₂O) and 180 mg of CO(NH₂)₂ was dissolved in 30 ml of distilled water under continuous magnetic stirring until a transparent wine color solution was formed. Then the reaction mixture was transferred in Teflon line-autoclave to treat it hydrothermally at 180 °C for 12 h. Subsequently the autoclave was cooled down to room temperature and the black precipitate was collected and washed with distilled water and ethanol respectively to remove the remnant and finally the sample was dried at 90 °C for further use. Finally it was calcinated at 300 °C for 3h to obtained the crystalline Co₃O₄.

Synthesis of CuS@Co₃O₄: The binary system was synthesized using a procedure similar to that used for the preparation of the ternary material, with the exception of the omission of g-C₃N₄.

Synthesis procedure of g-C₃N₄: g-C₃N₄ was prepared via a simple calcination method. Melamine (C₃N₃(NH₂)₃) was calcinated by muffled furnace at 620 °C. The yellow powder obtained was used for further studies and research purpose.

Table S1 PXRD Rietveld refined structural information of Co₃O₄, CuS, binary composite and ternary composite system.

Sample Composition	Phases with its phase fraction	Atom s	Wyckoff site	Positional parameters			Occupan cy	Bond length (Å)
				x	y	z		
Co ₃ O ₄	100% Pure cubic phase	Co1	8a	0.00000	0.00000	0.00000	1.00	(Co1–O1) = 1.933
		O1	32e	0.38810	0.38810	0.38810	1.00	(Co2–O1) = 1.92
		Co2	16d	0.62500	0.62500	0.62500	1.00	
	Crystal system = Cubic, lattice parameters: a = b = c = 8.08013 Å; α = β = γ = 90°; cell volume = 527.539 Å ³ , space group = Fd-3m (SG#227). R-Factors: R _p = 1.22, R _{wp} = 1.53, R _{exp} = 1.51, R _{Bragg} = 2.63, R _F = 3.63; χ ² = 1.02							
93.4% Hexago		Cu1	4f	0.33333	0.66667	0.10666	1.00	(Cu1–S1) = 2.32220
		Cu2	2d	0.33333	0.66667	0.75000	1.00	(Cu1–S2) = 2.3484
		S1	4e	0.00000	0.00000	0.05965	1.00	(Cu2–S2) = 2.19076

CuS	nal CuS phase	S2	2c	0.33333	0.66667	0.25000	1.00	
	Crystal system = Hexagonal, lattice parameters: $a = b = 3.79449 \text{ \AA}$, $c = 16.38446 \text{ \AA}$; $\alpha = \beta = 90^\circ$, $\gamma = 120^\circ$; cell volume = 204.288 \AA^3 , space group = P_{63}/mmc (SG #1194). R-Factors: $R_p = 1.73$, $R_{wp} = 2.31$, $R_{exp} = 1.82$, $R_{Bragg} = 1.25$, $R_F = 1.14$; $\chi^2 = 1.60$							
	6.6% Cubic Cu _{1.8} S phase	Cu1	8c	0.00000	0.00000	0.00000	1.00	(Cu1-S1) = 2.39996
	Cu2	32f	0.25000	0.25000	0.25000	0.496	(Cu2-S1) = 2.26436	
	S1	4a	0.32527	0.32527	0.32527	0.38		
Crystal system = Cubic, lattice parameters: $a = b = c = 5.54206 \text{ \AA}$; $\alpha = \beta = \gamma = 90^\circ$; cell volume = 170.221 \AA^3 , space group = $Fm-3m$ (SG#225). R-Factors: $R_{Bragg} = 0.56$, $R_F = 2.31$								
binary composite system	46.4% cubic Co ₃ O ₄ phase	Crystal system = Cubic, lattice parameters: $a = b = c = 8.08710 \text{ \AA}$; $\alpha = \beta = \gamma = 90^\circ$; cell volume = 528.907 \AA^3 , space group = $Fd-3m$ (SG#227). R-Factors: $R_p = 1.41$, $R_{wp} = 1.77$, $R_{exp} = 1.30$, $\chi^2 = 1.84$, $R_{Bragg} = 42.4$, $R_F = 51.9$.						
	44.5% Hexagonal CuS phase	Crystal system = Hexagonal, lattice parameters: $a = b = 3.79297 \text{ \AA}$, $c = 16.36940 \text{ \AA}$; $\alpha = \beta = 90^\circ$, $\gamma = 120^\circ$; cell volume = 203.950 \AA^3 , space group = P_{63}/mmc (SG #1194). R-Factors: $R_{Bragg} = 28.8$, $R_F = 27.5$.						
	9.1% Cubic Cu _{1.8} S phase	Crystal system = Cubic, lattice parameters: $a = b = c = 5.54412 \text{ \AA}$; $\alpha = \beta = \gamma = 90^\circ$; cell volume = 170.411 \AA^3 , space group = $Fm-3m$ (SG#225). R-Factors: $R_{Bragg} = 23.5$, $R_F = 70.1$						
CuS/Co ₃ O ₄ @ g-C ₃ N ₄ composite system	39.4% cubic Co ₃ O ₄ phase	Crystal system = Cubic, lattice parameters: $a = b = c = 8.12143 \text{ \AA}$; $\alpha = \beta = \gamma = 90^\circ$; cell volume = 535.671 \AA^3 , space group = $Fd-3m$ (SG#227). R-Factors: $R_p = 1.39$, $R_{wp} = 1.77$, $R_{exp} = 1.73$, $\chi^2 = 1.05$, $R_{Bragg} = 5.18$, $R_F = 5.92$.						

37.6% Hexagonal CuS phase	Crystal system = Hexagonal, lattice parameters: $a = b = 3.79642 \text{ \AA}$, $c = 16.41605 \text{ \AA}$; $\alpha = \beta = 90^\circ$, $\gamma = 120^\circ$; cell volume = 204.902 \AA^3 , space group = P_{63}/mmc (SG #1194). R-Factors: $R_{\text{Bragg}} = 4.39$, $R_F = 4.97$
23% Cubic $\text{Cu}_{1.8}\text{S}$ phase	Crystal system = Cubic, lattice parameters: $a = b = c = 5.54669 \text{ \AA}$; $\alpha = \beta = \gamma = 90^\circ$; cell volume = 170.648 \AA^3 , space group = $Fm-3m$ (SG#225). R-Factors: $R_{\text{Bragg}} = 5.28$, $R_F = 13.2$

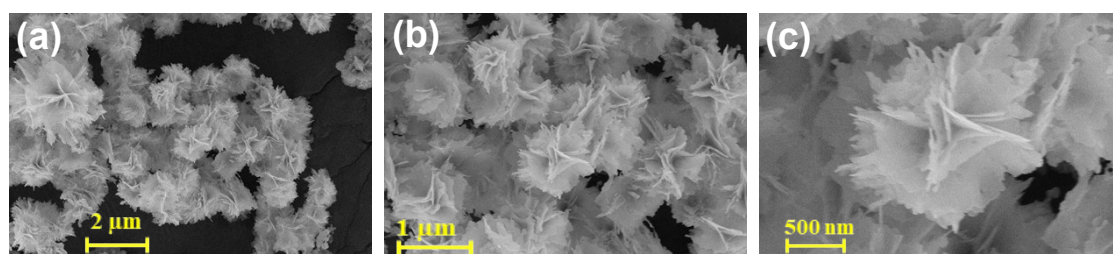


Fig. S1: (a-c) FESEM images of CuS pristine materials.

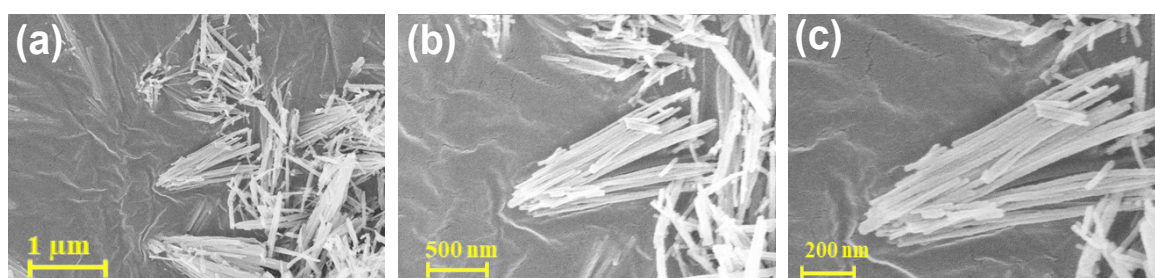


Fig. S2: (a-c) FESEM images of Co_3O_4 pristine materials.

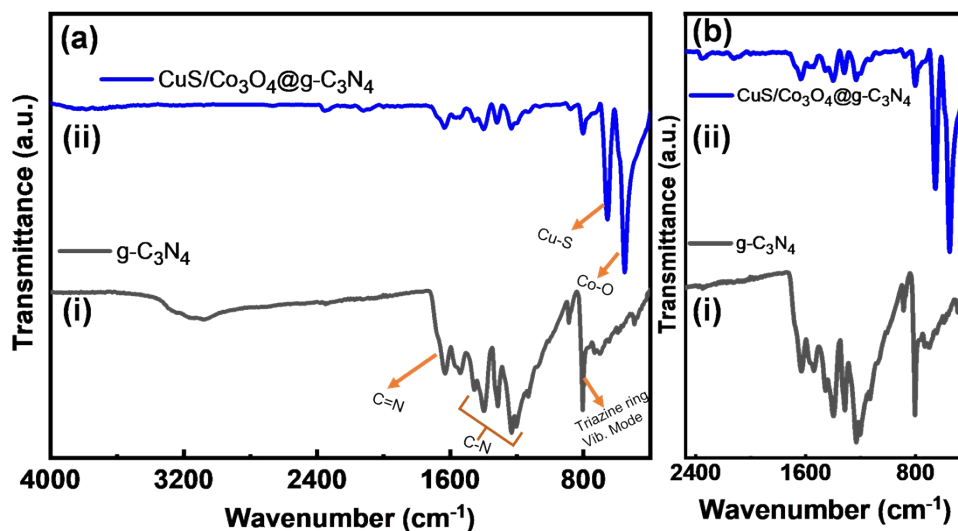


Fig. S3: ATR-FTIR spectra of ternary, binary and pristine Co_3O_4 , CuS and $\text{g-C}_3\text{N}_4$.

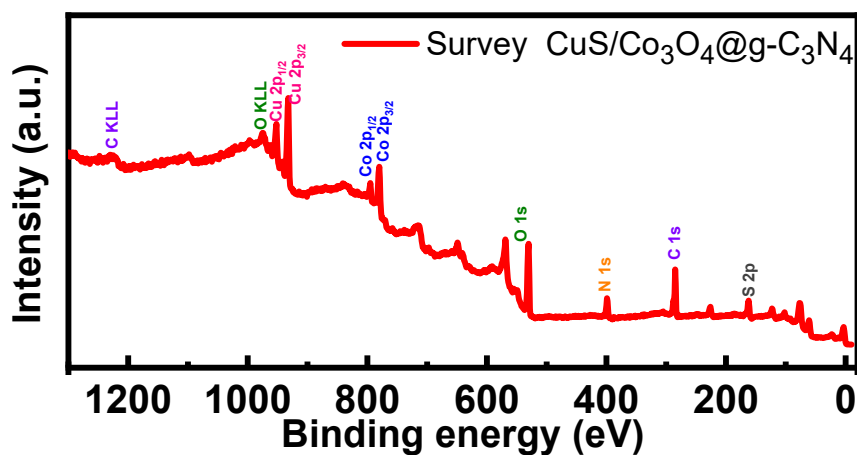


Fig. S4. XPS survey spectra of $\text{CuS/Co}_3\text{O}_4@\text{g-C}_3\text{N}_4$ ternary nanostructure.

Table S2. Mass activity results of ternary binary composite and all other pristine electrocatalyst.

S.No	Mass Activity		
	Electrocatalysts	OER	HER
1	Bare CC	8.99	4.9
2	$\text{g-C}_3\text{N}_4$	22.24	5.21
3	CuS	38.79	9.35
4	Co_3O_4	78.52	37.42
5	$\text{CuS/Co}_3\text{O}_4$	234.12	86.78
6	$\text{CuS/Co}_3\text{O}_4@\text{g-C}_3\text{N}_4$	462.56	165.43

Electrochemical surface area (ECSA):

The electrochemically active surface area (ECSA) is proportional to the electrochemical double layer capacitance (C_{dl}) and the ECSA can be calculated using the following equation.

$$ECSA = C_{dl}/C_s \dots \dots \dots (2)$$

Where C_s is the specific capacitance of flat working electrode and its value is $40 \mu\text{F cm}^{-2}$ ECSA for the flat electrode.^{1,2} The double-layer capacitance (C_{dl}) is calculated from the slope of anodic current density (J_a), cathodic current density (J_c) vs scan rate plot. The slope is directly proportion to the C_{dl} value.

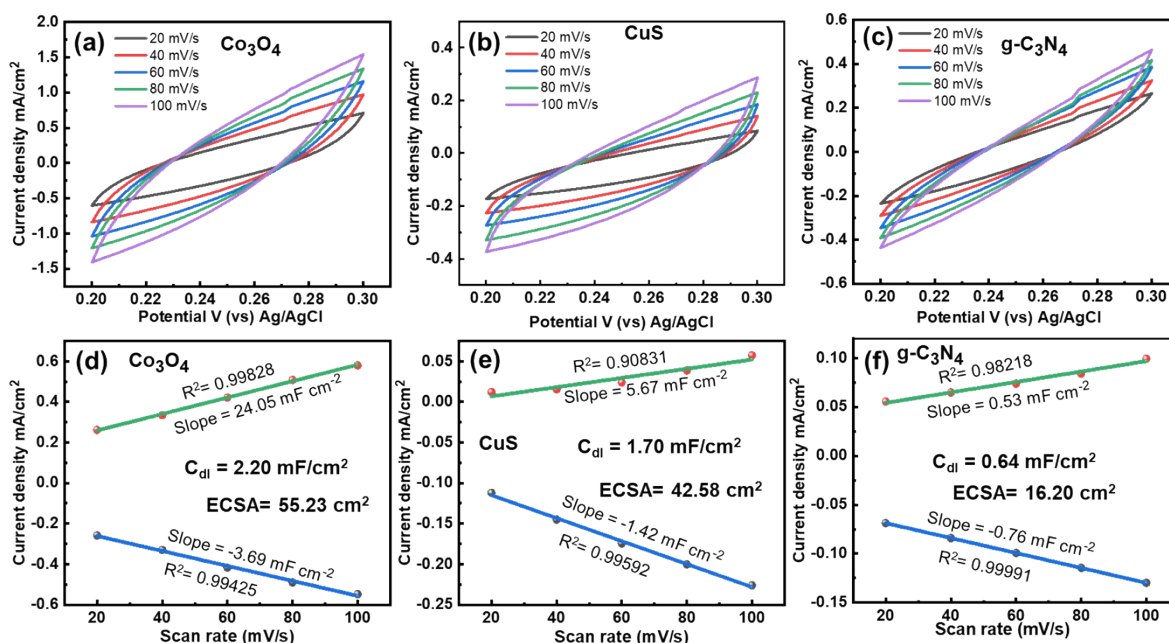


Fig. S5. Cyclic voltammograms of (a) pristine Co_3O_4 (b) pristine CuS (c) $\text{g-C}_3\text{N}_4$ composite (d-f) are their corresponding plot of J_a and J_c against scan rate for the determination of double layer capacitance (C_{dl}) of the catalysts, respectively.

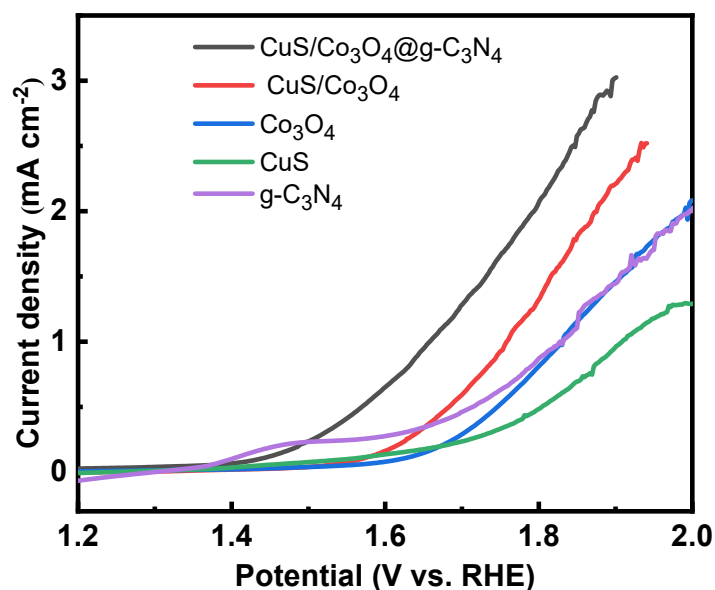


Fig. S6. ECSA Normalization from LSV in 1M KOH for OER.

Turnover Frequency (TOF) of all the electrocatalysts by using the following relation:

$$TOF = \frac{J \times NA}{n \times F \times \tau} \dots\dots (3)$$

Complete details are of catalysts of active sites (τ) TOF and are presented in textual part of manuscript and in Table S3 Fig. S7 & S8:

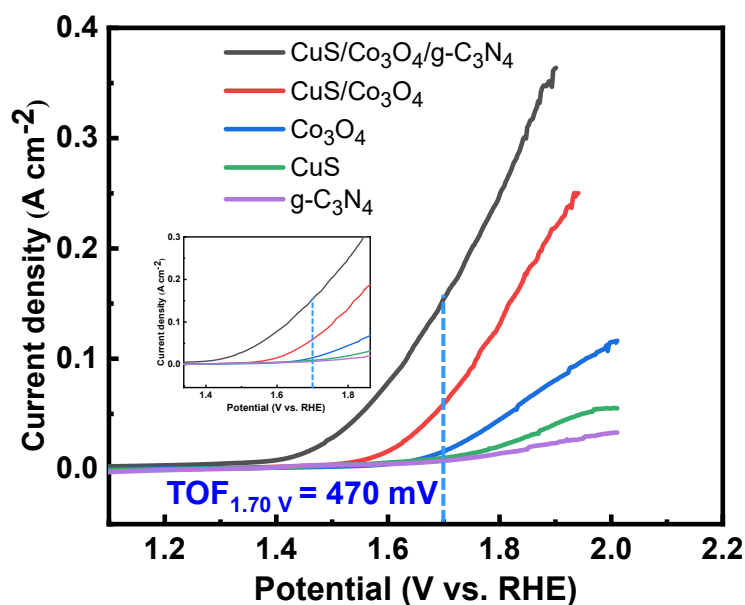


Fig. S7. TOF from LSV at voltage of 1.70 V (470 mV) and current density (in A/cm²) of CuS/Co₃O₄@g-C₃N₄, CuS/Co₃O₄, Co₃O₄, CuS and g-C₃N₄ only in 1M KOH for OER.

Active sites (τ) was calculated by the following equation:

$$\tau = \frac{\text{area of the } C_{dl}}{\text{Scan rate} \times 1.601 \times 10^{-19}} \dots\dots (1)$$

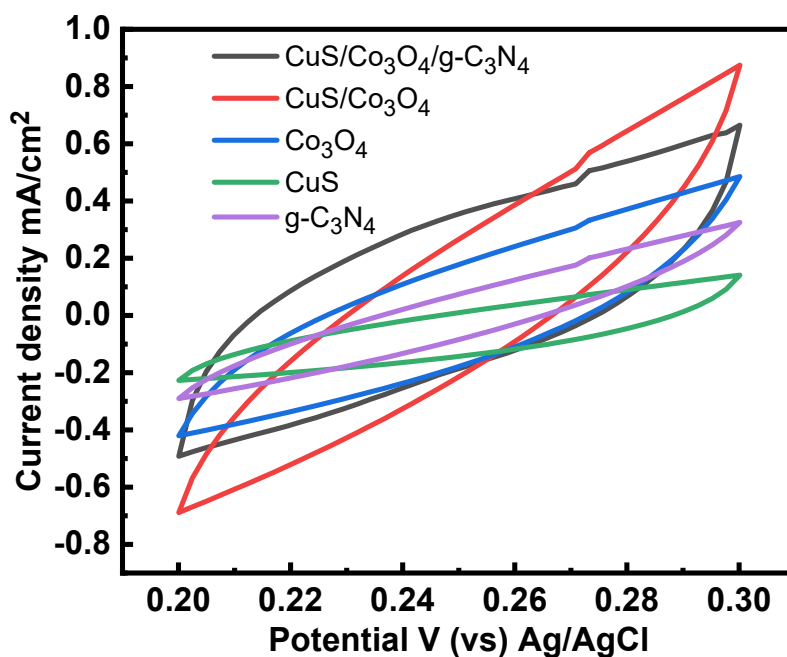


Fig. S8. CV curves of CuS/Co₃O₄@g-C₃N₄, CuS/Co₃O₄, Co₃O₄ CuS and g-C₃N₄ in 1 M KOH (pH ~ 13.8) solution in a given potential range of 0.2 V to 0.3 V (vs RHE) at a scan rate of 40 mV/s to enumerate the active sites.

Table S3. Active sites (τ) and TOF results of CuS/Co₃O₄@g-C₃N₄ CuS/Co₃O₄, Co₃O₄ CuS and g-C₃N₄ electrocatalyst.

S.No	Mass Activity		
	Electrocatalysts	Active sites (τ)	TOF
1	CuS/Co ₃ O ₄ @g-C ₃ N ₄	6.944×10^{15}	0.3438 s^{-1}
2	CuS/Co ₃ O ₄	5.854×10^{15}	0.1611 s^{-1}
3	Co ₃ O ₄	4.228×10^{15}	0.1446 s^{-1}
4	CuS	1.859×10^{15}	0.1101 s^{-1}
5	g-C ₃ N ₄	1.865×10^{15}	0.0511 s^{-1}

Table S4. Comparison of OER and HER activity of CuS/Co₃O₄@g-C₃N₄ ternary nanostructure with some reported copper and cobalt based catalysts in an alkaline medium and acidic medium.

Catalyst	Method of catalyst synthesis	Overpotential (mV) at 10 mA/cm ²		Tafel slope (mV dec ⁻¹)		Electrolyte used		Reference
		OER	HER	OER	HER	OER	HER	
Co ₃ O ₄ /NC/C	Thermal Decomp.	40		43 mV dec ⁻¹		1M KOH	3
CuFeS ₂ /rGO		176	153	216	150	1M KOH	1M KOH	4
Co ₃ O ₄ /C	Hydrothermal Approach	290	70		0.1 M KOH	5
g-C ₃ N ₄ /CeO ₂ /Fe ₃ O ₄	Hydrothermal Approach	400	310			1M KOH	1M KOH	6
Ni@CuS/SGCN	380		178		1M KOH	0.5 M H ₂ SO ₄	7
Co ₃ O ₄ @MoS ₂	Hydrothermal Approach	269	207	58	58	1M KOH	1 M KOH & 0.5M H ₂ SO ₄	8
rGO/MnO ₂ /MoS ₂	Hydrothermal Approach	208	205	73.7	76.13	1M KOH	1M KOH	9
Co ₃ O ₄ @NiO	Chemical growth method then calcination	330	101	1M KOH	10
Cu ₂ S NRs@CoS*	275	54	237	121	1M KOH	1M KOH	11
NiO@MoO ₃ /VC	Hydrothermal Approach	280	64.5	1M KOH	12
CoTe/MnO ₂ /BN	Hydrothermal Approach	273	81	1M KOH	13
ZnO/Co ₃ O ₄	Chemical Deposition	294	49	1M KOH	14
RGO/MoS ₂ /Pd	Hydrothermal Approach	245	86	42	35.9	1M KOH	1M KOH	15
RuO ₂ /Co ₃ O ₄	Co-precipitation	305	89	69	91	1M KOH	1 M KOH	16
Co/Co ₃ O ₄	Hydrother	129*	44	1 M KOH	17

	mal Approach							
Co ₃ O ₄ /MoO ₃ /g-C ₃ N ₄	Hydrothermal method	206	125	60	94	1M KOH	0.5 M H ₂ SO ₄	18
Cu ₂ S/MoS ₂ /CF	Hydrothermal method	91	41		1M KOH	19
CuS/Co₃O₄@g-C₃N₄	Hydrothermal Approach	191	78	213	89	1M KOH	0.5 M H₂SO₄	Present Work

Note: * = Overpotential at 50 mA cm⁻²

Table S5. Comparison of OER and HER chrono and LSV stability of some reported copper and cobalt based catalysts in an alkaline medium and acidic medium.

S. No	Catalysts	Electrolytes (HER/OER)	Chronoamperometry Stability (Time in hours)		LSV Polarization Stability (Cycles)		References
			HER	OER	HER	OER	
1	Co ₃ O ₄ /NC/C	1M KOH	20 h	100 h	1 st & 2000 th	3
2	g-C ₃ N ₄ /CeO ₂ /Fe ₃ O ₄	1M KOH	14 h	6
3	rGO/MnO ₂ /MoS ₂	1M KOH	12 h	12 h	9
4	Co ₃ O ₄ /MoO ₃ /g-C ₃ N ₄	0.5 M H ₂ SO ₄ /1M KOH	24 h	24 h	1 st & 3000 th	1 st & 3000 th	17
5	Cu ₂ S NRs@CoS	1M KOH	36 h	36 h	11
6	NiO@MoO ₃ /VC	1M KOH		15 h	500 th	12
7	CoTe/MnO ₂ /BN	1M KOH		24 h	2500 th	13
8	Cu ₂ S/MoS ₂ /CF	1M KOH	4 h	1000 th	19
9	CuS/Co₃O₄@g-C₃N₄	0.5 M H₂SO₄/1M KOH	40 h	60 h	1st & 2000th	1st & 2000th	This Work

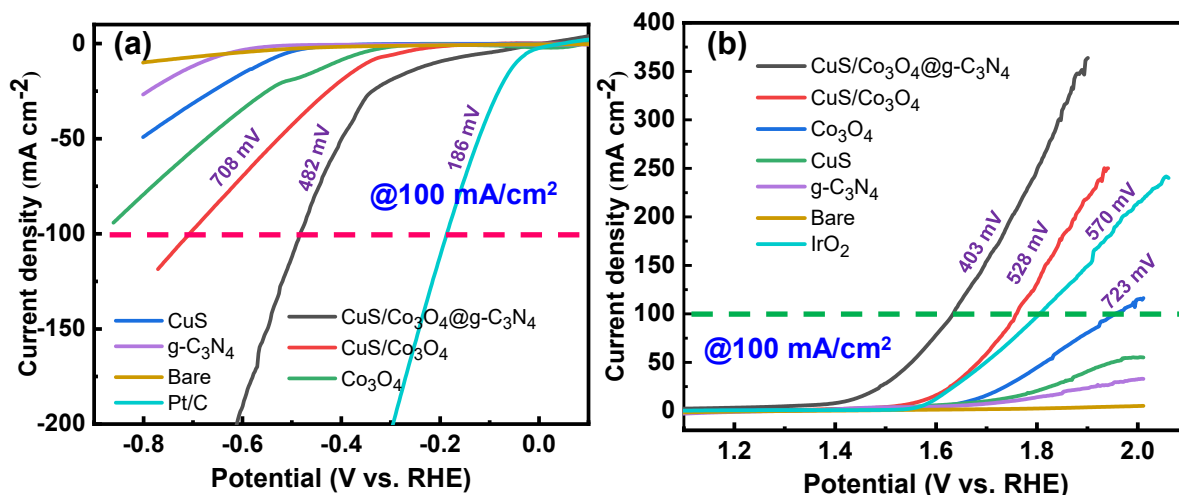
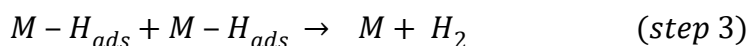
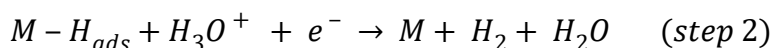
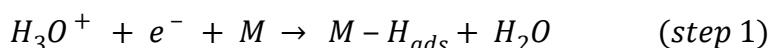


Fig. S9: Polarization curves (LSV) plot, representing the overpotential at higher current density (100 mA/cm^2) for both (a) HER and (b) OER for the electrocatalyst.

Most Possible Overall HER pathway:

HER process proceeds through three principal steps and they are called as Volmer, the Heyrovsky, and the Tafel steps, in acidic medium.²⁰⁻²³ Volmer reaction is associated with proton absorption which is a primary discharge step (Step 1). Heyrovsky step is the electrochemical desorption stage i.e., combination of a second proton with an adsorbed H atom of H_2 gas (step 2) where Tafel step is a recombination step i.e., the combination of two nearby adsorbed H atoms to produce H_2 gas (step 3).



Where H_{ads} represents a hydrogen atom chemically adsorbed on an active site of the catalyst surface (M). If Volmer reaction is the rate-determining step, then the Tafel slope should be 120 mV dec^{-1} , and for the Heyrovsky process and Tafel process, the Tafel slope of 40 and 30 mV dec^{-1} should be obtained, respectively.^{23, 24} So combinations of steps, i.e., Volmer-Heyrovsky or Volmer-Tafel pathway are required to produce molecular hydrogen in a complete HER process.

Most Possible Overall OER pathway:

The most possible overall OER pathway and the overall OER pathway under basic condition is described in our revised manuscript accordingly. At initial stage, active sites are reacted with the OH^- anion of the alkaline medium at the catalyst surface and started to form adsorbed OH^- species (stage 1). Afterwards, the adsorbed OH species further react with another OH^- ions to generate H_2O and adsorbed atomic O^* and discharge an electron (stage 2). Then, an OH^- anion reacts with an adsorbed O^* atom to produce adsorbed OOH species (stage 3). Moreover, further reaction with extra OH^- anions generates adsorbed O_2 and H_2O and after that adsorbed O_2 molecules were discharged finally in the stage (stage 4). All the steps associated in the reaction mechanism have been portrayed as follows:

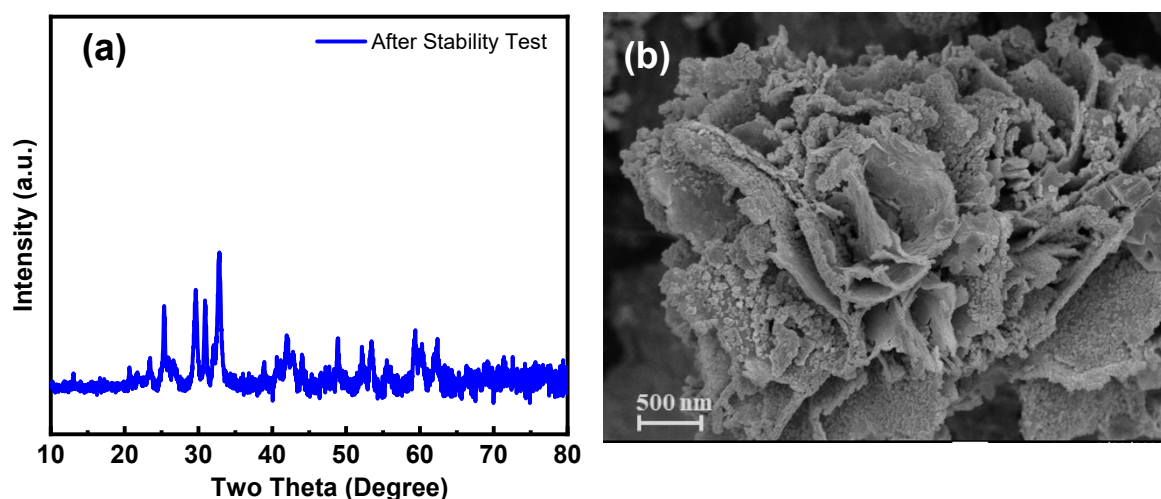
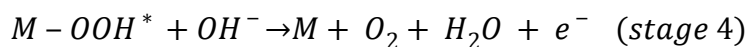
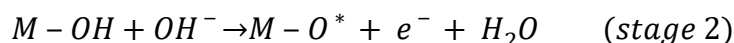
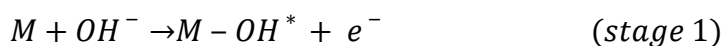


Fig. S10: Post catalytic XRD and FESEM analysis of $\text{CuS}/\text{Co}_3\text{O}_4/\text{g-C}_3\text{N}_4$ electrocatalyst after chronoamperometric stability test in 1 M KOH.

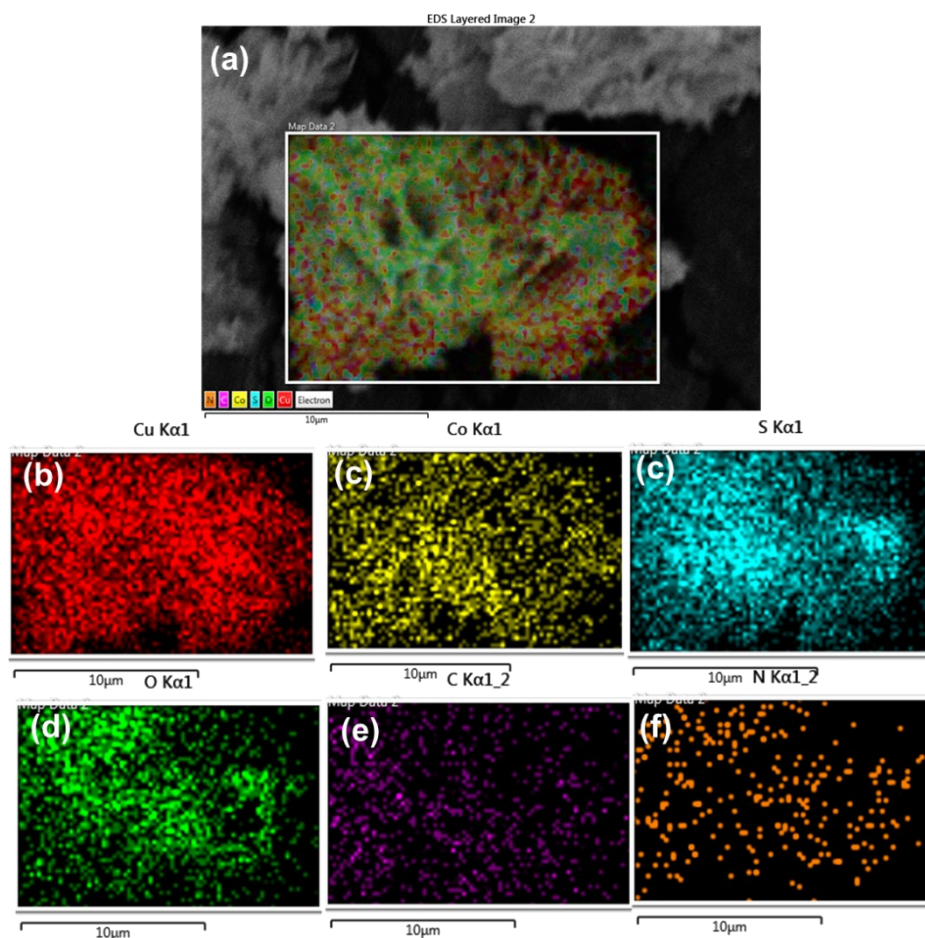


Fig. S11: Post catalytic mapping analysis of $\text{CuS}/\text{Co}_3\text{O}_4@\text{g-C}_3\text{N}_4$ electrocatalyst after chronoamperometric stability test in 1 M KOH.

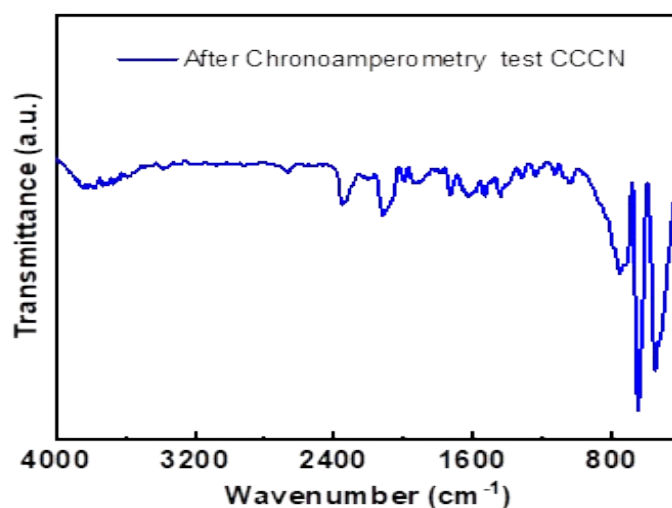


Fig. S12: Post catalytic ATR-FTIR of $\text{CuS}/\text{Co}_3\text{O}_4@\text{g-C}_3\text{N}_4$ electrocatalyst after chronoamperometric stability test in 1 M KOH.

References:

1. T. A. Ho, C. Bae, H. Nam, E. Kim, S. Y. Lee, J. H. Park, H. Shin *ACS Appl. Mater. Interfaces* 2018, **10**, 12807-12815.
2. Y. Li, F.-M. Li, X.-Y. Meng, S.-N. Li, J.-H. Zeng and Y. J. A. C. Chen, 2018, **8**, 1913-1920.
3. S. Du, Z. Ren, J. Zhang, J. Wu, W. Xi, J. Zhu and H. Fu, *Chem. Commun.*, 2015, **51**, 8066-8069.
4. S. Swathi, R. Yuvakkumar, G. Ravi, M. Thambidurai, H. D. Nguyen and D. Velauthapillai, *ACS Appl. Nano Mater.*, 2023, **6**, 6538-6549.
5. S. A. Needham, G. Wang, K. Konstantinov, Y. Tournayre, Z. Lao and H.-K. Liu, *Electrochem. and Solid State Lett.*, 2006, **9**, A315.
6. J. Rashid, N. Parveen, T. u. Haq, A. Iqbal, S. H. Talib, S. U. Awan, N. Hussain and M. Zaheer, *ChemCatChem*, 2018, **10**, 5587-5592.
7. M. Javed, M. A. Qamar, M. Shariq, I. A. Ahmed, K. B. Alziyadi, E. Almutib, A.-N. M. Alaghaz, R. Azooz and S. K. Ali, *J. of The Electrochem. Soc.*, 2023, **170**, 116506.
8. J. Liu, J. Wang, B. Zhang, Y. Ruan, H. Wan, X. Ji, K. Xu, D. Zha, L. Miao and J. Jiang, *J. Mater. Chem. A*, 2018, **6**, 2067-2072.
9. S. Denisdon, P. Senthil Kumar, C. Boobalan and G. Rangasamy, *Langmuir*, 2024, **40**, 17753-17766.
10. A. QayoomMugheri, U. Aftab, M. IshaqAbro, S. R. Chaudhry, L. Amaral and Z. H. Ibupoto, *Electrochim. Acta*, 2019, **306**, 9-17.
11. Q. Zhou, T.-T. Li, J. Wang, F. Guo and Y.-Q. Zheng, *Electrochim. Acta*, 2019, **296**, 1035-1041.
12. R. Illathvalappil, L. George and S. Kurungot, *ACS Appl. Energy Mater.* 2019, **2**, 4987-4998.
13. P. Rani, R. Biswas, A. Dutta and P. S. Alegaonkar, *Energy & Fuels*, 2024.
14. L. Zhang, H. Li, B. Yang, Y. Zhou, Z. Zhang and Y. Wang, *J. Solid State Electrochem.*, 2019, **23**, 3287-3297.
15. A. Pandey, A. Mukherjee, S. Chakrabarty, D. Chanda and S. Basu, *ACS Appl. Mater. & Interfaces*, 2019, **11**, 42094-42103.
16. H. Liu, G. Xia, R. Zhang, P. Jiang, J. Chen and Q. Chen, *RSC Adv.*, 2017.
17. X. Yan, L. Tian, M. He and X. Chen, *Nano Lett.*, 2015, **15**, 6015-6021.
18. I. Ahmed, R. Biswas, R. A. Patil, K. K. Halder, H. Singh, B. Banerjee, B. Kumar, Y.-R. Ma and K. K. Haldar, *ACS Appl. Nano Mater.*, 2021, **4**, 12672-12681.
19. X. Wang, J. Wang, X. Zhang, Q. Tian, M. Liu, N. Cai, Y. Xue, W. Chen, W. Li and F. Yu, *ChemCatChem*, 2019, **11**, 1354-1361.
20. N. Pentland, J. M. Bockris and E. Sheldon, *J. Electrochem. Soc.*, 1957, **104**, 182.
21. M. Basu, R. Nazir, C. Mahala, P. Fageria, S. Chaudhary, S. Gangopadhyay and S. Pande, *Langmuir*, 2017, **33**, 3178-3186.
22. B. Conway and B. Tilak, *Electrochim. Acta*, 2002, **47**, 3571-3594.
23. J. Xie, J. Zhang, S. Li, F. Grote, X. Zhang, H. Zhang, R. Wang, Y. Lei, B. Pan and Y. Xie, *J. Am. Chem. Soc.*, 2013, **135**, 17881-17888.
24. T. Hu, K. Bian, G. Tai, T. Zeng, X. Wang, X. Huang, K. Xiong and K. Zhu, *The J. Phys. Chem. C*, 2016, **120**, 25843-25850.